NUMERICAL MATHEMATICS: Theory, Methods and Applications
Numer. Math. Theor. Meth. Appl., Vol. **xx**, No. x, pp. 1-25 (200x)

Accelerated Non-overlapping Domain Decomposition Method for Total Variation Minimization

Xue Li[1], Zhenwei Zhang[1], Huibin Chang[2], Yuping Duan[1,*]

[1] *Center for Applied Mathematics, Tianjin University, Tianjin, 300072, China*
[2] *School of Mathematical Sciences, Tianjin Normal University, P.R. China.*

Abstract. We concern with fast domain decomposition methods for solving the total variation minimization problems in image processing. By decomposing the image domain into non-overlapping subdomains and interfaces, we consider the primal-dual problem on the interfaces such that the subdomain problems become independent problems and can be solved in parallel. Suppose both the interfaces and subdomain problems are uniformly convex, we can apply the acceleration method to achieve an $O(1/n^2)$ convergent domain decomposition algorithm. The convergence analysis is provided as well. Numerical results on image denoising, inpainting, deblurring, and segmentation are provided and comparison results with existing methods are discussed, which not only demonstrate the advantages of our method but also support the theoretical convergence rate.

Key words: Non-overlapping domain decomposition method, primal-dual algorithm, total variation, Rudin-Osher-Fatemi model, Chan-Vese model

1. Introduction

Minimizing the total variation (TV) was first proposed by Rudin, Osher and Fatemi in [29] for image denoising problem, and has captured wide attention due to its ability in preserving sharp edges and discontinuities when removes noises. Let Ω be an open bounded subset of $\mathbb{R}^n$ with Lipschitz continuous boundaries, $f : \Omega \to \mathbb{R}$ be a given image defined on the domain Ω, and $u : \Omega \to \mathbb{R}$ be the latent clean image. The generalized TV minimization model can be formulated to minimize the following energy functional

$$\min_{u\in \mathrm{BV}(\Omega)} \Big\{F(u) := \mathrm{TV}(u) + \frac{\lambda}{2}\int_\Omega (Au - f)^2 dx\Big\}, \tag{1.1}$$

where $\lambda \equiv \text{const} > 0$ is a weight parameter used to tradeoff between the data fidelity term and the regularization term, A is a linear and bounded operator varying with image

*Corresponding author. *Email addresses:* yuping.duan@tju.edu.cn

processing tasks, $\mathrm{BV}(\Omega)$ is the space of functions of bounded variation on Ω, and $\mathrm{TV}(u)$ stands for the total variation defined by

$$\mathrm{TV}(u) = \sup\left\{ \int_\Omega u \mathrm{div}\boldsymbol{p} dx : \boldsymbol{p} = (p_1, p_2) \in C_0^1(\Omega; \mathbb{R}^2), \|\boldsymbol{p}\|_\infty \leq 1 \right\}$$

with $C_0^1(\Omega, \mathbb{R}^2)$ being the space of continuously differentiable vector valued functions with compact support on Ω and $\|\boldsymbol{p}\|_\infty = \sup_x \sqrt{\sum_i p_i^2(x)}$.

Various numerical algorithms have been studied for solving the TV minimization problem, especially for the Rudin-Osher-Fatemi model, including the direct primal approaches such as the gradient descent method [29], fixed-point method [33], split Bregman iteration [18], and augmented Lagrangian method [34]. Chambolle [3] reformulated (1.1) by the Fenchel-Rockafellar dual and solved the dual problem by the semi-implicit gradient descent algorithm. Chambolle and Pock [4] considered the min-max optimization problem for solving the general problems in image processing, where the first-order primal-dual algorithm was developed for the nonlinear convex problem with an $O(1/n)$ convergent rate of convergence. What's more, as long as the minimization problem is uniformly convex, e.g., the Rudin-Osher-Fatemi model, it is shown that the $O(1/n^2)$ convergence rate can be achieved by updating the step sizes dynamically. Other methods for solving the model (1.1) include the fast non-iterative algorithm in [11], the primal-dual fixed-point algorithm in [9], the proximity algorithm in [27], and general Douglas-Rachford algorithms in [12], etc.

The aforementioned methods work well on small- and medium-scale image problems, but fail to address extremely large problems in realistic CPU-time such as traffic problems [32]. Domain decomposition methods (DDMs) [31, 35] can make use of distributed memory computers by breaking down the problem into a sequence of smaller scale subproblems and solve them in parallel. Over the past two decades, both overlapping and non-overlapping DDMs have been well studied for the variational model in image processing problems. Fornasier and Schönlieb [17] proposed a non-overlapping DDM algorithm for total variation minimization, the convergence of which was theoretically guaranteed. The idea was further studied for the case of overlapping DDM in [16]. Xu, Tai, and Wang [36] proposed a two-level overlapping DDM for the Rudin-Osher-Fatemi model by directly solving the nonlinear partial differential equation. Duan and Tai [15] developed an overlapping DDM for the Rudin-Osher-Fatemi model, where graph cuts were used to solve the subdomain minimization problem. To avoid the difficulties in minimizing the nonsmooth and nonadditive total variation term, the dual problem is considered to develop convergent DDM-based algorithms. Langer, Osher, and Schönlieb [21] developed a non-overlapping DDM by enforcing the restriction onto the respective subdomain by a Bregman iteration, which was subsequently solved by a split Bregman strategy. Hintermüller and Langer [19] considered the discrete dual Rudin-Osher-Fatemi model with a non-overlapping domain decomposition, where subproblems were solved by a semi-smooth Newton method. Chang *et al.* [8] analyzed the convergent rate of overlapping DDM for the dual Rudin-Osher-Fatemi model, where the subproblems were solved by the

semi-implicit gradient descent. Lee and Nam [22] developed a non-overlapping domain decomposition method for the total variation minimization problem based on dual decomposition. Langer and Gaspoz [20] presented sequential and parallel overlapping domain decomposition methods for the primal problem with a theoretical guarantee to converge to the minimizer of the global problem. Recently, Lee and Park [24] proposed the non-overlapping relaxed block Jacobi method for a dual formulation of the Rudin-Osher-Fatemi model and obtained an accelerated version with $O(1/n^2)$ convergent rate, which is the only $O(1/n^2)$ convergent DDM using the finite-difference discretization to our knowledge. Besides, convergent non-overlapping DDMs have been studied based on the primal-dual formulation of the total variation minimization problem. Duan, Chang, and Tai [14] proposed a non-overlapping DDM by formulating the constrained total variation model as a saddle-point problem, which was then solved by the primal-dual algorithm. Lee, Nam, and Park [23] transformed the total variation minimization with L^1 fidelity term into an equivalent saddle-point problem. By the dual conversion of total variation term on the subdomain interfaces, an equivalent saddle-point problem was obtained with parallel structures. We refer readers to [13, 25] for a thorough survey of the DDM algorithms for total variation minimization.

In this paper, we propose an accelerated non-overlapping DDM for the total variation minimization problems. Let the image domain be decomposed into non-overlapping subdomains and interfaces. We construct a parallel algorithm by solving the sub-minimization problems on subdomains and interfaces alternatively. The efficient Chambolle-Pock primal-dual algorithm is used to solve the sub-minimization problems on both subdomain and interface. We also discuss the convergence of the proposed DDMs theoretically. Inferred from the numerical experiments, our proposal is shown efficient and stable concerning image scales, subdomain numbers, and other model parameters. The main contributions of our work are summarized below

- We present an accelerated non-overlapping DDM for the Rudin-Osher-Fatemi model. Because both subdomain and interface minimization problems are uniformly convex, we can achieve a theoretical $O(1/n^2)$ convergent parallel algorithm;
- We develop an efficient non-overlapping DDM for the convex Chan-Vese model, where the sub-minimization problems on both subdomains and interfaces are solved by the Chambolle-Pock splitting method;
- We conduct numerous experiments to demonstrate the convergence and efficiency of our proposal. By compared with state-of-the-art non-overlapping DDMs, the proposed one presents significantly better convergence speed. Such a comparison study is important but neglected in the previous works.

This paper is organized as follows. In Sect. 2, we present the notations and revisit two non-overlapping DDMs developed based on the primal-dual formulation of the total variation minimization. Sect. 3 is dedicated to develop an accelerated non-overlapping DDM for the Rudin-Osher-Fatemi model, in which an $O(1/n^2)$ convergence rate is achieved theoretically. We design an efficient non-overlapping DDM for the convex Chan-Vese model

in Sect. 4. Intensive numerical experiments on image denoising, inpainting, deblurring, and segmentation are provided to verify the advantages of the proposed DDM in Sect. 5. We conclude the paper with some remarks in Sect. 6.

2. Preliminaries

In this section, we introduce some basic notations in the discrete setting and review two related non-overlapping DDMs for the total variation minimization problems.

2.1. Notations

Without loss of generality, we define the domain Ω for the images of the resolution $M \times N$ as follows

$$\Omega = [1, 2, \ldots, M] \times [1, 2, \ldots, N].$$

We denote V and V^* as spaces of functions from Ω into $\mathbb{R}$ and $\mathbb{R}^2$, respectively. Then for a given pixel point $(i, j) \in \Omega$, we denote $u(i, j) \in \mathbb{R}$ and $\boldsymbol{p}(i, j) = (p_1(i, j), p_2(i, j)) \in \mathbb{R}^2$ for $u \in V$ and $\boldsymbol{p} \in V^*$, respectively. We equip V and V^* with the standard Euclidean inner products

$$\langle u, v \rangle_V = \sum_{i,j} u(i, j)v(i, j) \quad \text{and} \quad \langle \boldsymbol{p}, \boldsymbol{q} \rangle_{V^*} = \langle p_1, q_1 \rangle_V + \langle p_2, q_2 \rangle_V,$$

and the induced norms

$$\|u\|_V = \sqrt{\langle u, u \rangle_V} \quad \text{and} \quad \|\boldsymbol{p}\|_{V^*} = \sqrt{\langle \boldsymbol{p}, \boldsymbol{p} \rangle_{V^*}}.$$

Without ambiguity, we omit the subscripts V and V^* below. The discrete forward and backward differential operators for $u \in V$ are defined with the homogeneous Neumann boundary condition as follows

$$\partial_x^+ u(i, j) = \begin{cases} u(i+1, j) - u(i, j), & 1 \le i < M, \\ 0, & i = M, \end{cases}$$

$$\partial_y^+ u(i, j) = \begin{cases} u(i, j+1) - u(i, j), & 1 \le j < N, \\ 0, & j = N, \end{cases}$$

$$\partial_x^- u(i, j) = \begin{cases} u(i, j), & i = 1, \\ u(i, j) - u(i-1, j), & 1 < i < M, \\ -u(i-1, j), & i = M, \end{cases}$$

$$\partial_y^- u(i, j) = \begin{cases} u(i, j), & j = 1, \\ u(i, j) - u(i, j-1), & 1 < j < N, \\ -u(i, j-1), & j = N. \end{cases}$$

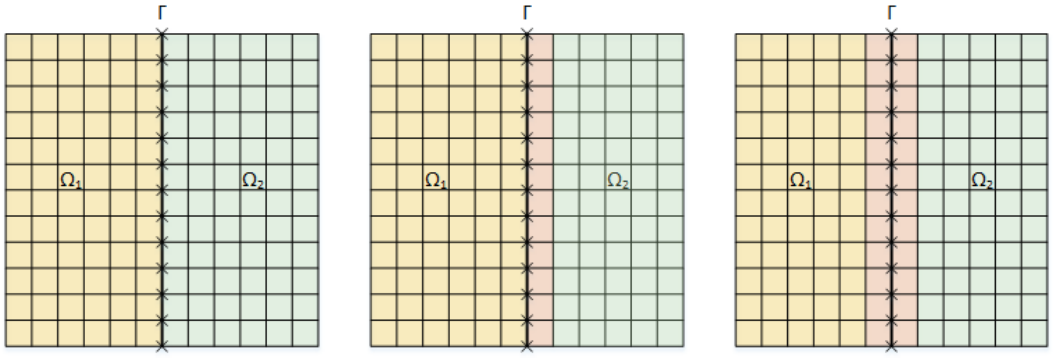

(a) Type I (b) Type II (c) Type III

Figure 2.1: Three non-overlapping domain decomposition methods using the stripe-type decomposition.

The discrete gradient operator $\nabla : V \to V^*$ is defined for $u \in V$ as

$$\nabla u(i,j) = (\partial_x^+ u(i,j), \partial_y^+ u(i,j)),$$

and the discrete total variation is defined as the 1-norm of ∇u for $u \in V$

$$\|\nabla u\|_1 = \sum_{i,j} |\nabla u(i,j)|,$$

where $|\nabla u(i,j)| = \sqrt{(\partial_x^+ u(i,j))^2 + (\partial_y^+ u(i,j))^2}$. Besides, the discrete divergence is defined by the duality relationship between the divergence and the gradient, i.e., $\mathrm{div} = -\nabla^*$. For $\boldsymbol{p} \in V^*$, there is

$$\mathrm{div}\boldsymbol{p}(i,j) = \partial_x^- p_1(i,j) + \partial_y^- p_2(i,j).$$

We also define the local notations for the domain decomposition methods. Supposing that S is a subset of Ω, i.e., $S \subset \Omega$, we denote $u|_S(i,j) = u(i,j)$ for $(i,j) \in S$ and $u|_S(i,j) = 0$ otherwise. Note that $u|_S$ is different from u_S, where the latter one is a new variable independent of u. Similarly, we define the local gradient operator on S as $\nabla_S u(i,j) = \nabla u(i,j)$ for $(i,j) \in S$, and $\nabla_S u(i,j) = 0$ otherwise. It is easy to induce the local divergence $-\nabla_S^*$ by the duality relationship. More generally, for a linear operator K defined on Ω, we define K_S by $K_S u = (Ku)|_S$. Hereafter, we save the trouble of defining the same operators with different subscripts whenever there is no ambiguity.

2.2. Non-overlapping DDMs based on the primal-dual formulation

We use a simple example with two subdomains to illustrate different ways to define the non-overlapping domain decomposition; see Figure 2.1. As shown, image domain Ω is decomposed into two subsets Ω_1, Ω_2 and the interface Γ. More specifically, we use the column marked with "×" to denote the interface Γ, and yellow and green color to denote the subdomain Ω_1 and Ω_2, respectively. The red region indicates the boundary between

the interface and subdomain, where $\Gamma \subset \Omega_1$ and $\Gamma \subset \Omega_2$ for type I, $\Gamma \subset \Omega_1$ and $\Gamma \not\subset \Omega_2$ for type II, and $\Gamma \not\subset \Omega_1$ and $\Gamma \not\subset \Omega_2$ for type III.

2.2.1. Duan-Chang-Tai method

Duan *et al.* [14] developed a non-overlapping domain decomposition method for the convex Chan-Vese model

$$\min_{0\le u\in V\le 1} F(u) := \langle u, h\rangle + \lambda\|\nabla u\|_1, \tag{2.1}$$

where $h = (f-c_0)^2 - (f-c_1)^2$ is defined by the input image f and the mean values of the foreground c_0 and background c_1. Referring to Figure 2.1 (a), the decomposition satisfies $\Gamma = \Omega_1 \cap \Omega_2$, and $\Omega = \Omega_1 \cup \Omega_2$. By introducing an equivalent constraint on the interface, the original minimization problem (2.1) is reformulated into the following saddle-point problem

$$\begin{aligned} \min_{0\le u_i\in V_i\le 1} \quad & \mathrm{F}_1(u_1) + \mathrm{F}_2(u_2) \\ \text{s.t.,} \quad & u_1 = u_2 \text{ on } \Gamma, \end{aligned} \tag{2.2}$$

where

$$\mathrm{F}_1(u_1) = \lambda\|\nabla_{\Omega_1\setminus\Gamma} u_1\|_1 + \langle u, h|_{\Omega_1\setminus\Gamma}\rangle \quad \text{and} \quad \mathrm{F}_2(u_2) = \lambda\|\nabla_{\Omega_2} u_2\|_1 + \langle u, h|_{\Omega_2}\rangle,$$

with $V_i = \{u \in V \mid \mathrm{supp(u)} \subset \Omega_i\}$ for $i = 1, 2$. By introducing a Lagrangian multiplier $g \in V_\Gamma := \{g \in V \mid \mathrm{supp(g)} \subset \Gamma\}$, the following saddle-point problem is built up

$$\min_{0\le u_i\in V_i\le 1} \max_{g\in V_\Gamma} \sum_{i=1}^{2} \mathrm{F}_i(u_i) + \langle u_1 - u_2, g\rangle, \tag{2.3}$$

which is solved by the Chambolle-Pock primal-dual algorithm [4]. The specific non-overlapping DDM algorithm is described as Algorithm Duan16.

Algorithm Duan16 in [14]

---

1. Initialization:choose $g^0 = 0$, $u_i^0 = \bar{u}_i^0 = 0$, and select parameters τ, σ and $\theta \in [0, 1]$;
2. Iterations to update u_i^{n+1}, g^{n+1}, $\bar{u}_i^{n+1}$ for $n = 0, 1, 2, \cdots$

$$\begin{aligned} g^{n+1} &= g^n + \sigma(\bar{u}_1^n - \bar{u}_2^n)|_\Gamma; \\ (\tilde{u}_1^n, \tilde{u}_2^n) &= (u_1^n, u_2^n) - \tau(g^{n+1}, -g^{n+1}); \\ (u_1^{n+1}, u_2^{n+1}) &= \arg\min_{0\le u_i\in V_i\le 1} \sum_{i=1}^{2} \left(F_i(u_i) + \frac{1}{2\tau}\|u_i - \tilde{u}_i^n\|^2 \right); \\ \bar{u}_i^{n+1} &= (1+\theta)u_i^{n+1} - \theta u_i^n; \end{aligned}$$

3. End till some stopping criterion is met.

2.2.2. Lee-Nam-Park method

In [23], Lee, Nam and Park proposed a domain decomposition method using the dual conversion locally for total variation minimization with the L^1 data fidelity term for impulsive noise removal. As shown in Figure 2.1 (b), the two subdomains satisfy that $\Omega_1 \cap \Omega_2 = \emptyset$, and the interface satisfies $\Gamma \subset \Omega_1$ and $\Gamma \notin \Omega_2$. To be specific, the following saddle-point problem is concerned with

$$\min_{u\in V} \max_{\boldsymbol{p}_\Gamma \in V^*} \langle \nabla_\Gamma u, \boldsymbol{p}_\Gamma \rangle - I_\chi(\boldsymbol{p}_\Gamma) + \lambda \|u - f\|_1 + \|\nabla_{\Omega_1\setminus\Gamma} u\|_1 + \|\nabla_{\Omega_2} u\|_1, \tag{2.4}$$

where $I_\chi(\cdot)$ denotes the characteristic function of the set $\chi = \{\boldsymbol{p} \mid |\boldsymbol{p}(i,j)| \le 1,\ \forall\, (i,j) \in \Omega\}$. By the dual conversion on the interfaces, the saddle-point problem has a parallel structure. The resulting non-overlapping DDM is referred to as Algorithm Lee19 hereafter, where $V_i = \{u \in V \mid \mathrm{supp(u)} \subset \Omega_\mathrm{i}\}$ for $i = 1,\ 2$.

Algorithm Lee19 in [23]

---

1. Initialization: choose $\tau,\ \sigma > 0$ with $\tau\sigma < 1/||\nabla_\Gamma||^2$, $\theta \in [0,1]$, and $\bar{u}^0 = u^0 = 0,\ \boldsymbol{p}_\Gamma^0 = \boldsymbol{0}$;

2. Iterations to update the variables $\boldsymbol{p}^{n+1}$ and u^{n+1} for $n = 0, 1, 2, \cdots$

$$\begin{aligned}
&\tilde{\boldsymbol{p}}_\Gamma^{n+1} = \boldsymbol{p}_\Gamma^n + \sigma \nabla_\Gamma \bar{u}^n;\\
&\boldsymbol{p}_\Gamma^{n+1} = \frac{\tilde{\boldsymbol{p}}_\Gamma^{n+1}}{\max\{1, |\tilde{\boldsymbol{p}}_\Gamma^{n+1}|\}};\\
&\tilde{u}^{n+1} = u^n - \tau \nabla_\Gamma^* \boldsymbol{p}_\Gamma^{n+1};\\
&u_1^{n+1} = \arg\min_{u_1 \in V_1} \|\nabla_{\Omega_1\setminus\Gamma} u_1\|_1 + \lambda \|u_1 - f|_{\Omega_1}\|_1 + \frac{1}{2\tau}\|u_1 - \tilde{u}^{n+1}|_{\Omega_1}\|^2;\\
&u_2^{n+1} = \arg\min_{u_2 \in V_2} \|\nabla_{\Omega_2} u_2\|_1 + \lambda \|u_2 - f|_{\Omega_2}\|_1 + \frac{1}{2\tau}\|u_2 - \tilde{u}^{n+1}|_{\Omega_2}\|^2;\\
&u^{n+1} = u_1^{n+1} + u_2^{n+1};\\
&\bar{u}^{n+1} = (1+\theta)u^{n+1} - \theta u^n;
\end{aligned}$$

3. End till some stopping criterion is met.

---

3. The accelerated non-overlapping DDM for the Rudin-Osher-Fatemi model

In this section, we propose an accelerated non-overlapping DDM for the Rudin-Osher-Fatemi denoising model, in which A is an identity operator. The image domain is decomposed as Figure 2.1 (c), where $\Omega_1 \cap \Omega_2 = \emptyset$, $\Gamma \notin \Omega_1$ and $\Gamma \notin \Omega_2$. The interface Γ is defined

as follows

$$\Gamma = [1, 2, \cdots, M] \times [N_1],$$

and the resulting two non-overlapping subdomains are given as

$$\begin{aligned}\Omega_1 &= [1, 2, \cdots, M] \times [1, 2, \cdots, N_1 - 1],\\ \Omega_2 &= [1, \cdots, M] \times [N_1 + 1, \cdots, N].\end{aligned}$$

Furthermore, we define

$$\bar{\Omega}_1 = [1, 2, \cdots, M] \times [1, 2, \cdots, N_1], \quad \bar{\Omega}_2 = \Omega_2, \quad \bar{\Gamma} = [1, 2, \cdots, M] \times [N_1, N_1 + 1].$$

The corresponding local function spaces for the subdomains are given as follows

$$\begin{aligned} V_1 &= \{u \in V \mid \mathrm{supp}(u) \subset \bar{\Omega}_1\}, & V_1^* &= \{\boldsymbol{p} \in V^* \mid \mathrm{supp}(\boldsymbol{p}) \subset \Omega_1\},\\ V_\Gamma &= \{u \in V \mid \mathrm{supp}(u) \subset \bar{\Gamma}\}, & V_\Gamma^* &= \{\boldsymbol{p} \in V^* \mid \mathrm{supp}(\boldsymbol{p}) \subset \Gamma\},\\ V_2 &= \{u \in V \mid \mathrm{supp}(u) \subset \bar{\Omega}_2\}, & V_2^* &= \{\boldsymbol{p} \in V^* \mid \mathrm{supp}(\boldsymbol{p}) \subset \Omega_2\}. \end{aligned}$$

Thus, there is $V = V_1 + V_\Gamma + V_2$ and $V^* = V_1^* \oplus V_\Gamma^* \oplus V_2^*$. Now, we propose the new non-overlapping DDM algorithm by rewriting the minimization problem (1.1) as follows

$$\min_{u \in V} \ \|\nabla_\Gamma u\|_1 + \|\nabla_{\Omega_1} u\|_1 + \|\nabla_{\Omega_2} u\|_1 + \frac{\lambda}{2}\|u - f\|^2. \tag{3.1}$$

By pursuing the primal-dual formulation on Γ, we consider the following saddle-point problem

$$\min_{u \in V} \max_{\boldsymbol{p}_\Gamma \in V_\Gamma^*} \ \mathscr{L}(u, \boldsymbol{p}_\Gamma) = \langle \nabla_\Gamma u, \boldsymbol{p}_\Gamma \rangle - \underbrace{I_\chi(\boldsymbol{p}_\Gamma)}_{H^*(\boldsymbol{p})} + \underbrace{\frac{\lambda}{2}\|u - f\|^2}_{G(u)} + \underbrace{\sum_{i=1}^{2} \|\nabla_{\Omega_i} u\|_1}_{J(u)}. \tag{3.2}$$

Then we can define the sub-minimization problems on Ω_i as follows

$$\mathrm{F}_i(u_i) := \underbrace{\frac{\lambda}{2}\|u_i - f|_{\Omega_i}\|^2}_{G_i(u_i)} + \underbrace{\|\nabla_{\Omega_i} u_i\|_1}_{J_i(u_i)}, \qquad \text{for } \ i = 1, 2,$$

which are separable and can be solved in parallel. Here the main difference between our splitting and the one in [23] is the treatment on the fidelity term. Specifically, we solve a complete Rudin-Osher-Fatemi model (1.1) on Γ, while only total variation term is minimized on Γ in [23]. The merit of bundling the fidelity term and total variation together is to achieve a better convergence rate on the interface. Because the L^2 fidelity term is strongly convex, we can apply the acceleration technique to the saddle-point problem on Γ and achieve an $O(1/n^2)$ convergence rate [1, 28]. The detailed non-overlapping DDM is stated as Algorithm 1, where $PD_{\tau_n,\sigma_n}(u^n, \boldsymbol{p}_\Gamma^n, \bar{u}^n)$ denotes the saddle-point problem on the interface.

Algorithm 1 Accelerated non-overlapping DDM for image denoising

1. Initialization: choose $\tau_0, \sigma_0 > 0$ such that $\tau_0\sigma_0 < 1/\|\nabla_\Gamma\|^2$, and $\theta_0 = 0$, $\bar{u}^0 = u^0 = 0$, $\boldsymbol{p}_\Gamma^0 = \mathbf{0}$;

2. Iterations to update the variables u^{n+1} and $\boldsymbol{p}_\Gamma^{n+1}$ for $n = 0, 1, 2, \cdots$

$$
\begin{aligned}
&(\tilde{u}^{n+1}, \boldsymbol{p}_\Gamma^{n+1}) = PD_{\tau_n,\sigma_n}(u^n, \boldsymbol{p}_\Gamma^n, \bar{u}^n);\\
&(u_1^{n+1}, u_2^{n+1}) = \arg\min_{u_i \in V_i} \sum_{i=1}^{2} \left(F_i(u_i) + \frac{1}{2\tau_n} \|u_i - \tilde{u}^{n+1}|_{\tilde{\Omega}_i}\|^2 \right);\\
&u^{n+1} = u_1^{n+1} + \tilde{u}^{n+1}|_\Gamma + u_2^{n+1};\\
&\bar{u}^{n+1} = u^{n+1} + \theta_n(u^{n+1} - u^n);\\
&\theta_{n+1} = 1/\sqrt{1+\mu\tau_n}, \quad \tau_{n+1} = \theta_{n+1}\tau_n, \quad \sigma_{n+1} = \sigma_n/\theta_{n+1};
\end{aligned}
$$

3. End till some stopping criterion is met.

Now we discuss how to solve the local minimization problems on the interface and subdomains, respectively.

3.1. Local minimization problems on interfaces

The minimization problem on the interface is solved by the following primal-dual algorithm, where only values of u^n on $\bar{\Gamma}$ are updated and stored in $\tilde{u}^{n+1}$.

Interface Algorithm: $(\tilde{u}^{n+1}, \boldsymbol{p}_\Gamma^{n+1}) = PD_{\tau_n,\sigma_n}(u^n, \boldsymbol{p}_\Gamma^n, \bar{u}^n)$

1. Compute the dual variable $\boldsymbol{p}_\Gamma^{n+1}$ by

$$\boldsymbol{p}_\Gamma^{n+1} = I_\chi(\boldsymbol{p}_\Gamma^n + \sigma_n \nabla_\Gamma \bar{u}^n); \tag{3.3}$$

2. Update the primal variable $\tilde{u}^{n+1}$ on $\bar{\Gamma}$ from

$$\tilde{u}^{n+1} = \frac{u^n|_{\bar{\Gamma}} - \tau_n \nabla_\Gamma^* \boldsymbol{p}_\Gamma^{n+1} + \tau_n \lambda f|_\Gamma}{1 + \tau_n\lambda} + u^n|_{\Omega\setminus\bar{\Gamma}}. \tag{3.4}$$

3.2. Local minimization problem on subdomains

By introducing the dual variable of the local total variation, we can reformulate the minimization problem on subdomains into the following min-max problem

$$(u_i^{n+1}, \boldsymbol{p}_i^{n+1}) = \arg\min_{u_i \in V_i} \max_{\boldsymbol{p}_i \in V_i^*} \langle \nabla_{\Omega_i} u_i, \boldsymbol{p}_i \rangle - I_\chi(\boldsymbol{p}_i) + G_i(u_i) + \frac{1}{2\tau_n} \|u_i - \tilde{u}^{n+1}|_{\tilde{\Omega}_i}\|^2. \quad (3.5)$$

Note that the subdomain problems are solver-independent such that any existing total variation minimization algorithm can be applied with little modification. Because $G_i(u_i)$ is strongly convex for the denoising problem, the saddle-point problem (3.5) can be solved by the accelerated algorithms with the $O(1/n^2)$ convergence rate, such as fast iterative shrinkage-thresholding algorithm [1], accelerated linearized primal-dual algorithm [10], and accelerated primal-dual algorithm in [5]. In our paper, we follow [5] to solve the sub-minimization problems by the primal-dual algorithm as provided below.

Algorithm 2 Primal-dual algorithm on subdomains

---

1. Initialization: choose $\gamma_0 = \tau_n$, $\kappa_0 \gamma_0 = 1/L^2$, and $\theta_0 = 0$;
2. Iterations to update the variables u_i^{k+1} and $\boldsymbol{p}_i^{k+1}$ for $k = 0, 1, 2, \cdots, k_{max}$

$$\begin{aligned}
&\boldsymbol{p}_i^{k+1} = I_\chi(\boldsymbol{p}_i^k + \kappa_k \nabla_{\Omega_i} \bar{u}_i^k);\\
&u_i^{k+1} = \frac{\tau_n u_i^k - \tau_n \gamma_k \nabla_{\Omega_i}^* \boldsymbol{p}_i^{k+1} + \tau_n \gamma_k \lambda f|_{\Omega_i} + \gamma_k \tilde{u}^{n+1}|_{\tilde{\Omega}_i}}{\tau_n + \gamma_k + \tau_n \gamma_k \lambda};\\
&\bar{u}_i^{k+1} = u_i^k + \theta_k (u_i^{k+1} - u_i^k);\\
&\theta_{k+1} = 1/\sqrt{1 + \mu\gamma_k};\ \ \gamma_{k+1} = \theta_{k+1}\gamma_k;\ \ \kappa_{k+1} = \kappa_k/\theta_{k+1};
\end{aligned}$$

3. Return: $u_i^{n+1} = u_i^{k_{max}}|_{\Omega_i}$ and $\boldsymbol{p}_i^{n+1} = \boldsymbol{p}_i^{k_{max}}$.

There are two remarks for the implementation of Algorithm 2. Firstly, for saving the computational costs of local problems, u_i and $\boldsymbol{p}_i$, i=1, 2, are initialized using the values from the latest outer iteration. Secondly, the initialization for κ_0 and γ_0 can be chosen according to the discussion in [5], such that

$$\gamma_0 = 1/L_G = \tau_n, \quad \kappa_0 = L_G/L^2,$$

with $L = \|\nabla\| \leq \sqrt{8}$ and L_G being the Lipschitz constant of $G_i(u_i)$.

3.3. Convergence

Both our algorithms for the interface problems and subdomain problems are the convex-concave saddle-point problems discussed by Chambolle and Pock, the convergence of

which has been provided as Theorem 4 in [5]. Similar to [23], we directly offer the following theorems to demonstrate the convergence of the proposed Algorithm 1 and subdomain Algorithm 2.

Theorem 3.1. *Let $\{(u^n, \boldsymbol{p}_\Gamma^n)\}$ be the sequence generated by Algorithm 1. For $\tau_0 > 0$, $\tau_0\sigma_0 \leq 1/||\nabla_\Gamma||^2$, there exists a saddle-point $(u^*, \boldsymbol{p}_\Gamma^*)$ such that $(u^n, \boldsymbol{p}_\Gamma^n) \to (u^*, \boldsymbol{p}_\Gamma^*)$ as $n \to \infty$. Furthermore, the primal-dual gap*

$$\max_{\boldsymbol{p}_\Gamma \in V_\Gamma^*} \mathscr{L}(u_n, \boldsymbol{p}_\Gamma) - \min_{u \in V} \mathscr{L}(u, \boldsymbol{p}_{\Gamma,n})$$

tends to 0 in the rate of $O(1/n^2)$, where $u_n = \frac{1}{n}\sum_{i=1}^n u^i$ and $\boldsymbol{p}_{\Gamma,n} = \frac{1}{n}\sum_{i=1}^n \boldsymbol{p}_\Gamma^i$.

Proof. It is easy to prove that ∇_Γ is a bounded linear operator in the finite dimension space, and $\|\nabla_\Gamma\|^2 \leq \|\nabla\|^2 \leq 8$ refereed to [3]. Because G is strongly convex function and H^* and J are proper, lower semi-continuous, convex functions, one readily proves the theorem according to Theorem 4 in [5]. ■

Theorem 3.2. *The Algorithm 2 for solving the subdomain problems converges if $\gamma_0\kappa_0 \leq 1/8$.*

Proof. The proof is the same as Theorem 3.1. ■

4. The efficient non-overlapping DDM for the convex Chan-Vese model

We further consider the implementation of the non-overlapping DDM on the convex Chan-Vese model [6, 7] defined as

$$\min_{0 \leq u \in V \leq 1} \lambda\|\nabla u\|_1 + \langle 1 - u, C_s\rangle + \langle u, C_t\rangle, \tag{4.1}$$

where $C_s = (f - c_0)^2$ and $C_t = (f - c_1)^2$. Many efficient algorithms have been developed for solving the Chan-Vese model (4.1) such as the dual method [2], the Douglas-Rachford primal-dual [26], the continuous max-flow [37], and the Chambolle-Pock primal-dual [14], etc. Here, we follow the formulation of continuous max-flow model by considering the following saddle-point problem

$$\min_{u \in V} \max_{p_s, p_t \in V, \boldsymbol{p} \in V^*} \langle u, \mathrm{div}\boldsymbol{p} - p_s + p_t\rangle + \langle 1, p_s\rangle - I_{C_s}(p_s) - I_{C_t}(p_t) - I_\zeta(\boldsymbol{p}), \tag{4.2}$$

where $\zeta = \{\boldsymbol{p} \mid |\boldsymbol{p}(i,j)| \leq \lambda,\ \forall\ (i,j) \in \Omega\}$, and the projections $I_{C_s}(\cdot)$ and $I_{C_t}(\cdot)$ mean $\min\{\cdot, C_s\}$ and $\min\{\cdot, C_t\}$, respectively. In order to establish the convergence result, we group the dual variables together as $y = (\boldsymbol{p}, p_t, p_s)^T$, and define the linear operator K as $K = (-\nabla, I, -I)^T$. The above min-max problem (4.2) can be rewritten as follows

$$\min_{0 \leq u \in V \leq 1} \max_{y \in V^* \times V \times V} \langle Ku, y\rangle - H^*(y), \tag{4.3}$$

with

$$H^*(y) = -\langle 1, p_s\rangle + I_{C_t}(p_t) + I_{C_s}(p_s) + I_\zeta(\boldsymbol{p}).$$

By considering the primal-dual formulation on Γ, we can obtain an equivalent saddle-point problem with the parallel structure as follows

$$\min_{u\in V}\max_{y_\Gamma\in V_\Gamma^*\times V_\Gamma\times V_\Gamma} \mathscr{L}(u, y_\Gamma) = \langle K_\Gamma u, y_\Gamma\rangle - H^*(y_\Gamma) + \underbrace{\sum_{i=1}^{2}\Big(\langle 1-u, C_s|_{\Omega_i}\rangle + \langle u, C_t|_{\Omega_i}\rangle\Big)}_{G(u)} + \underbrace{\sum_{i=1}^{2}\lambda\|\nabla_{\Omega_i}u\|_1}_{J(u)},$$

where $y_\Gamma = \Big(\boldsymbol{p}_\Gamma, p_{t\Gamma}, p_{s\Gamma}\Big)^T$ and the sub-minimization problem can be defined as

$$F_i(u_i) := \underbrace{\langle 1-u_i, C_s|_{\Omega_i}\rangle + \langle u_i, C_t|_{\Omega_i}\rangle}_{G_i(u_i)} + \underbrace{\|\nabla_{\Omega_i}u_i\|_1}_{J_i(u_i)}, \qquad \text{for } i = 1, 2.$$

Then the corresponding non-overlapping DDM for the Chan-Vese model can be sketched as Algorithm 3.

Algorithm 3 Non-overlapping DDM for the Chan-Vese model

1. Initialization: choose $\tau,\ \sigma > 0$ such that $\tau\sigma < 1/\|K_\Gamma\|^2$, $\theta = 1$, and $\bar{u}^0 = u^0 = 0,\ y_\Gamma^0 = 0$;
2. Iterations to update the variables u^n and y_Γ^n for $n = 0, 1, 2, \cdots$

$$\begin{aligned}
(\tilde{u}^{n+1}, y_\Gamma^{n+1}) &= PD_{\tau,\sigma}(u^n, y_\Gamma^n, \bar{u}^n);\\
(u_1^{n+1}, u_2^{n+1}) &= \arg\min_{u_i\in V_i}\sum_{i=1}^{2}\left(F_i(u_i) + \frac{1}{2\tau}\left\|u_i - \tilde{u}^{n+1}|_{\bar{\Omega}_i}\right\|^2\right);\\
u^{n+1} &= u_1^{n+1} + \tilde{u}^{n+1}|_\Gamma + u_2^{n+1};\\
\bar{u}^{n+1} &= u^{n+1} + \theta(u^{n+1} - u^n);
\end{aligned}$$

3. End till some stopping criterion is met.

4.1. Local minimization on interfaces

It is easy to verify that all the variables can be solved by closed-form solutions with low costs. In particular, the corresponding Chambolle-Pock algorithm for the sub-minimization problem on interfaces is presented as follows.

Interface Algorithm: $(\tilde{u}^{n+1}, y_\Gamma^{n+1}) = PD_{\tau,\sigma}(u^n, y_\Gamma^n, \bar{u}^n)$

1. Estimate y_Γ^{n+1} by

$$\begin{aligned} \boldsymbol{p}_\Gamma^{n+1} &= I_\zeta(\boldsymbol{p}_\Gamma^n + \sigma\nabla_\Gamma \bar{u}^n); \\ p_{s\Gamma}^{n+1} &= I_{C_s}(p_{s\Gamma}^n + \sigma(1-\bar{u}_\Gamma^n)); \\ p_{t\Gamma}^{n+1} &= I_{C_t}(p_{t\Gamma}^n + \sigma\bar{u}_\Gamma^n); \end{aligned}$$

2. Update $\tilde{u}^{n+1}$ on $\bar{\Gamma}$ from

$$\tilde{u}^{n+1} = u^n - \tau K_\Gamma^* y_\Gamma^{n+1}.$$

4.2. Local minimization on subdomains

The solution of local problems on subdomains are formally in accord with the one on Γ, which solves the following saddle-point problem

$$(u_i^{n+1}, y_i^{n+1}) = \arg\min_{u_i\in V_i} \max_{y_i\in V_\Gamma^*\times V_\Gamma\times V_\Gamma} \langle Ku_i, y_i\rangle - H^*(y_i) + \frac{1}{2\tau_n}\left\|u_i - \tilde{u}^{n+1}|_{\bar{\Omega}_i}\right\|^2,$$

where the sub-minimization problems of the dual variable $y_i = \left(\boldsymbol{p}_i, p_{ti}, p_{si}\right)^T$ are the same as the one on the interfaces, and the sub-minimization problem of the primal variable contains another proximal term defined on $\bar{\Omega}_i$. Thus, the Chambolle-Pock algorithm for solving the local minimization on subdomains can be easily deduced as Algorithm 4.

Algorithm 4 Primal-dual algorithm on subdomains

1. Initialization: choose $\kappa, \gamma > 0$ such that $\kappa\gamma < 1/\|K\|^2$, and $\theta = 1$;

2. Iterations to update u_i^{k+1} and y_i^{k+1} for $k = 0, 1, 2, \cdots, k_{max}$

$$\begin{aligned} \boldsymbol{p}_i^{k+1} &= I_\zeta(\boldsymbol{p}_i^k + \kappa\nabla_{\Omega_i}\bar{u}_i^k); \\ p_{si}^{k+1} &= I_{C_s}\left(p_{si}^k + \kappa(1-\bar{u}_i^k)\right); \\ p_{ti}^{k+1} &= I_{C_t}(p_{ti}^k + \kappa\bar{u}_i^k); \\ u_i^{k+1} &= \frac{\gamma\tilde{u}^{n+1}|_{\bar{\Omega}_i} + \tau u_i^k - \gamma\tau(-\nabla_{\Omega_i}^*\boldsymbol{p}_i^{k+1} + p_{ti}^{k+1} - p_{si}^{k+1})}{\gamma+\tau}; \\ \bar{u}_i^{k+1} &= u_i^{k+1} + \theta(u_i^{k+1} - u_i^k); \end{aligned}$$

4. Return: $u_i^{n+1} = u_i^{k_{max}}|_{\Omega_i}$ and $y_i^{n+1} = y_i^{k_{max}}$.

4.3. Convergence

Similarly to [23], we can present the following theorems for the convergence of Algorithm 3 and Algorithm 4.

Theorem 4.1. *Let $\{(u^n, y_\Gamma^n)\}$ be the sequence generated by Algorithm 3. For $\theta = 1$, $\tau > 0$, and $\tau\sigma \leq 1/||K_\Gamma||^2$, there exists a saddle-point (u^*, y_Γ^*) such that $(u^n, y_\Gamma^n) \to (u^*, y_\Gamma^*)$ as $n \to \infty$. Furthermore, the primal-dual gap*

$$\max_{y_\Gamma \in V_\Gamma^*} \mathscr{L}(u_n, y_\Gamma) - \min_{u \in V} \mathscr{L}(u, y_{\Gamma,n})$$

tends to 0 in the rate of $O(1/n)$, where $u_n = \frac{1}{n}\sum_{i=1}^n u^i$ and $y_{\Gamma,n} = \frac{1}{n}\sum_{i=1}^n y_\Gamma^i$.

Proof. Since $K = \left(-\nabla, I, -I\right)^T$, we have $\|K_\Gamma\|^2 \leq \|K\|^2 \leq (\|\nabla\|^2 + 2) \leq 10$. Since G is a proper, continuous and convex function, and H^* and J are proper, lower semi-continuous convex functions, we can achieve the convergence with the rate $O(1/n)$ according to Theorem 1 in [5]. ■

Theorem 4.2. *The Algorithm 4 for solving the subdomain problems converges if $\gamma_0\kappa_0 \leq 1/10$.*

5. Numerical Experiments

In this section, we exhibit the numerical performances of our algorithm by applying it to various image processing tasks and comparing the performance with state-of-the-art non-overlapping DDMs.

5.1. Image reconstruction

In this subsection, we apply Algorithm 1 to denoising, inpainting, and deblurring problems, where A is an identity matrix, diagonal matrix with either 0 or 1, and convolution matrix with a size of 3×3 blurring kernel, respectively.

We start with denoising problems to evaluate the influences of the step sizes, the numerical convergence, and the efficiency of the proposed Algorithm 1. Two images "Boat" (512×512) and "Building" (1024×1024) are used in our numerical experiments for the denoising problem; see Figure 5.1, where the two images are degenerated by Gaussian white noise with mean 0 and variance 0.005 and variance 0.02, respectively. We use the stripe-shaped decomposition and the Peak Signal-to-Noise Ratio (PSNR) to measure the denoising performance. The absolute error of energy (E_n) and relative error (e_n) are adopted to terminate the external loops and internal loops, which are defined as

$$E_n = \frac{|F(u^n) - F(u^*)|}{F(u^*)}, \quad \text{and} \quad e_n = \frac{\|u^{n+1} - u^n\|^2}{\|u^{n+1}\|^2},$$

respectively, with u^* being the solution of the full size problem obtained by Algorithm 2 in [4] for 10^6 iterations. Here, $F(u^*)$ and $F(u^n)$ denote the numerical energy of u^* and u^n, respectively.

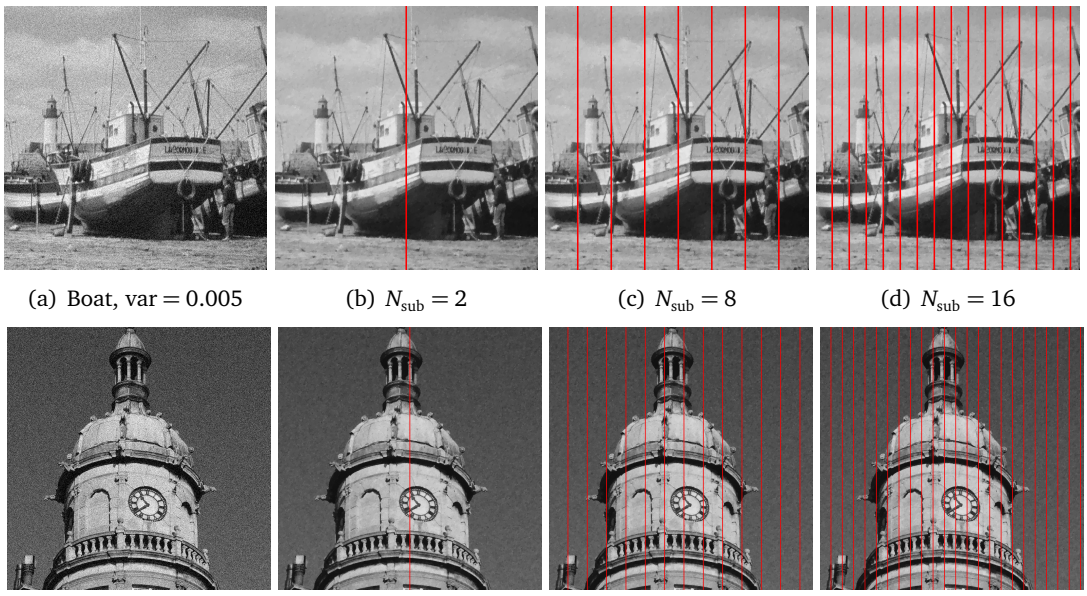

(a) Boat, var = 0.005 (b) $N_{\text{sub}} = 2$ (c) $N_{\text{sub}} = 8$ (d) $N_{\text{sub}} = 16$

(e) Building, var = 0.02 (f) $N_{\text{sub}} = 2$ (g) $N_{\text{sub}} = 14$ (h) $N_{\text{sub}} = 24$

Figure 5.1: Testing images for denoising and the corresponding denoising results using proposed non-overlapping DDM, where the red lines indicate the positions of interfaces Γ.

Firstly, we explore the influences of the initial step size τ_0 on the performance of Algorithm 1 with the fixed λ. We set the number of subdomains as $N_{\text{sub}} = 12$ and $N_{\text{sub}} = 16$ for image "Boat" and "Building", respectively, and we always keep the product of the two step sizes of the dual and primal variables as $1/8$ for both the external loops or the inner loops. Note that the same values are taken in the following tests unless otherwise specified. The number of inner iterations for the subdomain problems is fixed as 100. We find that increasing the number of iterations on Γ can effectively reduce the number of iterations on the outer loop, where the iteration for the dual variable on the interface problem is fixed as 20 iterations. As shown in Figure 5.2, the number of iterations required to reach the second-order convergence rate gradually decreases as τ_0 increases from 0.001 to 0.1. However, it does not mean the larger the τ_0 is, the better the convergence is. We observe that the convergence rate with $\tau_0 = 0.1$ is no more faster than the one with $\tau_0 = 0.01$ after the first few hundreds of iterations. Therefore, we take $\tau_0 = 0.05$ as the default value in the following experiments.

In practical applications, it is unreasonable to fix the number of inner iterations to be a large value, because the inner iterations converge faster and faster as the external loops proceed. Meanwhile, from the perspective of parallelism, it is also unwise to set the number of inner loops too small or solely use relative error to break off, because the fewer inner iterations usually lead to more external iterations and result in the rise of communication cost. In the case of parallel computing, the wall-clock time consumed is mainly composed of two parts, one is the communication time between the various subsystems, and the other is the time consumed to solve the sub-problems. It is worth

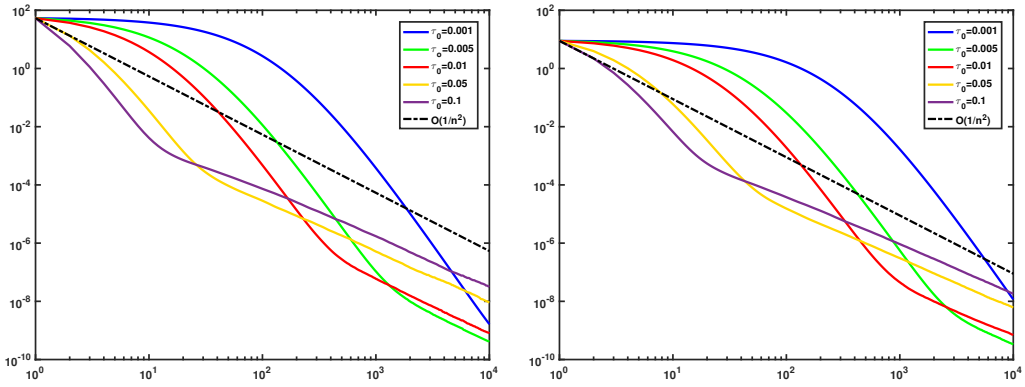

(a) Boat with $\lambda = 20$ (b) Building with $\lambda = 10$

Figure 5.2: Performance comparison of Algorithm 1 on image "Boat" and "Building" with different values of τ_0.

Table 5.1: The results of image "Boat" and "Building" with different numbers of inner iterations.

nIn	Boat,$\tau_0 = 0.05, \lambda = 20$				Building,$\tau_0 = 0.05, \lambda = 10$			
	Energy	Max_diff	Time	Iter	Energy	Max_diff	Time	Iter
1	18146.3103	0.0003	2.73	2497	107052.9514	0.0012	9.07	4095
5	18146.3102	0.0016	1.00	172	107052.9518	0.0024	2.37	224
10	18146.3102	0.0017	1.58	160	107052.9518	0.0028	3.92	188
20	18146.3103	0.0018	2.78	156	107052.9518	0.0030	6.85	174
50	18146.3103	0.0018	6.84	155	107052.9519	0.0031	15.87	168
100	18146.3102	0.0018	13.55	155	107052.9521	0.0032	31.60	167

noting that, although the algorithm we designed is communication-saving, the solving speed of the sub-problems is not guaranteed to be consistent. Therefore, the first part of the time is mainly the idle time, that is, the time difference between the fastest completed sub-problem and the slowest completed sub-problem. To minimize the idle time, we need to ensure the efficiency and speed consistency of each sub-problem solution at the same time. To that end, we exhibit the results of two testing images in Table 5.1, with respect to different numbers of inner iterations (nIn). The external loops of image "Boat" and "Building" are terminated by $E_n \leq 10^{-6}$ and $E_n \leq 5 \times 10^{-7}$, respectively. The "Time" in the tables refers to virtual wall-clock time, which is measured with the assumption that the algorithm is parallelized, i.e., we take the maximum value among wall-clock times consumed in all subdomains of each external iteration. The "Max_diff" is the maximum residual error defined as $\max|u^\diamond - u^*|$, where $u^\diamond$ is the solution obtained by our algorithm. The "Energy" in the tables refers to the value of the object energy functional when the algorithm converges, i.e., $F(u^\diamond)$. It is obviously shown that the number of external iteration decreases as we increase nIn from 1 to 10, but the downward trend becomes insignificant as nIn keeps increasing. We also observe that both PSNR and numerical energy remain the same as the number of inner iterations increases. We then simply let nIn $= 10$ for

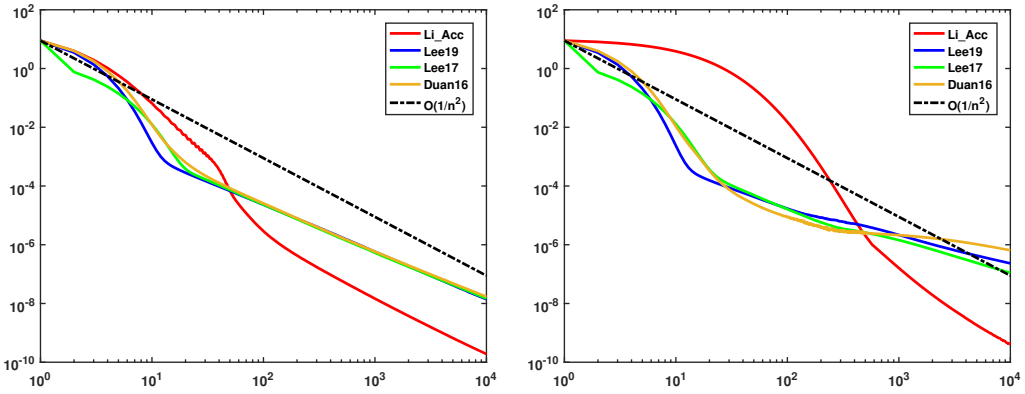

(a) Building with $nIn = 10$ (b) Building with $e_n \leq 10^{-6}$

Figure 5.3: Energy decay $E_n = \frac{F(u^n)-F(u^*)}{F(u^*)}$ of state-of-the-art non-overlapping DDM algorithms on image "Building".

denoising problems to balance the number of external iterations and time consumed on subdomains.

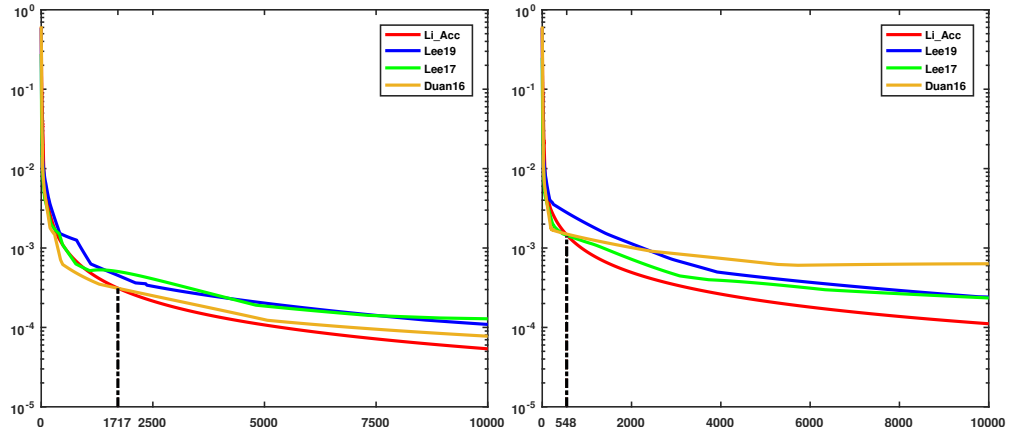

(a) Building with $nIn = 10$ (b) Building with $e_n \leq 10^{-6}$

Figure 5.4: The Max_diff decay of the different algorithms w.r.t. image "Building".

Now we compare the proposed Algorithm 1 (denoted as Li_Acc) with the other three non-overlapping DDMs Duan16 [14], Lee19 [23], and the relaxed block Jacobi algorithm (denoted as Lee17) [22]. We initialize the step sizes of algorithm Duan16 and Lee19 with $\tau = \gamma_0 = 0.05$ for a fair comparison. For algorithm Lee17, only local problems contain the step size parameter, which is set as $\gamma_0 = 0.05$. The local problems defined on subdomains of all comparison algorithms are solved by Algorithm 2 in [4], where $\mu = 0.7\lambda$ is chosen for all algorithms. Two terminating conditions of the inner loops are tested for the algorithms, i.e., nIn $= 10$ and $e_n \leq 10^{-6}$, illustrated in Figure 5.3(a) and Figure 5.3(b), respectively. Similar to the previous comparison, we plot the absolute errors of the numerical energy

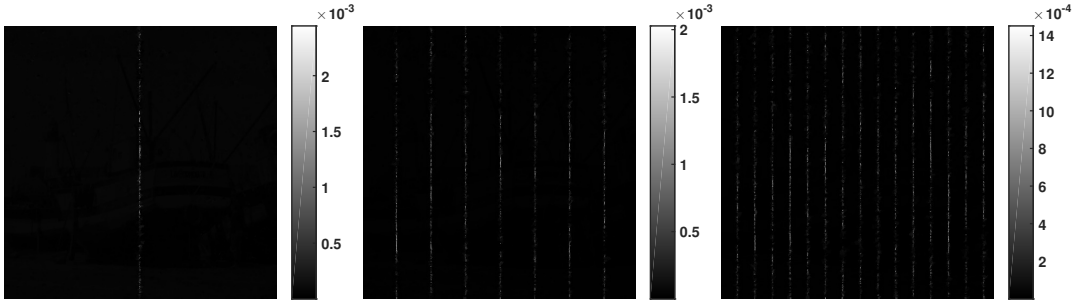

(a) $N_{\text{sub}} = 2$ (b) $N_{\text{sub}} = 8$ (c) $N_{\text{sub}} = 16$

Figure 5.5: Residual error of "Boat" with various numbers of sundomains.

obtained by the DDMs together with the theoretical $O(1/n^2)$ rate in Figure 5.3. As can be seen, the algorithm Duan16, Lee17, and Lee19 converge faster than our algorithm Li_Acc at the early stage, but the advantage of our method becomes significant as the number of iteration keeps increasing. It is effortless to notice that our non-overlapping DDM can achieve the second-order convergence rate under both termination conditions. In particular, our algorithm can achieve the desired convergence rate within one hundred iterations in Figure 5.3(a), which obviously outperforms the others in numerical convergence.

Table 5.2: Comparison results on image "Boat" with different numbers of subdomains.

N_{sub}	PSNR	Li_Acc,$\tau_0 = 0.05, \lambda = 10$				Lee19, $\tau = 0.05, \lambda = 20$			
		Energy	Max_diff	Time	Iter	Energy	Max_diff	Time	Iter
2	30.01	18146.3102	0.0024	5.99	85	18146.3103	0.0006	26.19	327
4	30.01	18146.3100	0.0026	1.28	104	18146.3103	0.0008	9.65	397
6	30.01	18146.3102	0.0022	1.05	116	18146.3103	0.0010	8.42	563
8	30.01	18146.3102	0.0020	0.99	133	18146.3103	0.0008	7.34	638
10	30.01	18146.3102	0.0019	0.98	148	18146.3103	0.0005	6.75	691
12	30.01	18146.3102	0.0017	0.97	160	18146.3103	0.0008	7.25	828
14	30.01	18146.3103	0.0016	0.94	167	18146.3103	0.0005	7.04	885
16	30.01	18146.3103	0.0015	0.92	181	18146.3103	0.0007	7.55	962

We also evaluate the performance of our method and Lee19 with respect to different numbers of subdomains. The results are displayed in Table 5.2 and Table 5.3, where the termination conditions are determined as $E_n \leq 10^{-6}$ and $E_n \leq 5 \times 10^{-7}$ for image "Boat" and "Building", respectively. From both tables, one readily knows that both algorithms demand more iterations to reach the same error tolerance as the number of subdomains increases. Obviously, our DDM always requires fewer iterations and is more stable concerning with the number of subdomains. We note that Algorithm Lee19 outperforms our proposal in terms of Max_diff. In order to investigate the reason, we plot the Max_diff decay curves of image "Building" in Figure 5.4, where the subdomain problems are terminated by either iteration number in Figure 5.4(a) or relative error in Figure 5.4(b). As can be seen, when both the step sizes and the number of subdomains are fixed, the Max_diff monotonically decreases as the number of iterations increases for all DDMs, and our al-

Table 5.3: Comparison results on image "Building" with different numbers of subdomains.

N_{sub}	PSNR	Li_Acc, $\tau_0 = 0.05,\ \lambda = 10$				Lee19, $\tau = 0.05,\ \lambda = 10$			
		Energy	Max_diff	Time	Iter	Energy	Max_diff	Time	Iter
2	27.91	107052.9517	0.0033	40.50	134	107052.9522	0.0004	205.45	643
4	27.91	107052.9514	0.0039	21.17	142	107052.9522	0.0008	112.05	732
6	27.91	107052.9513	0.0033	14.75	148	107052.9522	0.0006	81.75	826
8	27.91	107052.9515	0.0031	11.64	154	107052.9522	0.0009	65.63	899
10	27.91	107052.9519	0.0036	3.67	162	107052.9522	0.0007	34.67	982
12	27.91	107052.9518	0.0032	3.16	172	107052.9522	0.0008	29.66	995
14	27.91	107052.9522	0.0028	2.76	175	107052.9522	0.0007	32.25	1116
16	27.91	107052.9518	0.0028	2.51	188	107052.9522	0.0006	26.25	1141
18	27.91	107052.9521	0.0032	2.39	192	107052.9522	0.0007	19.88	1205
20	27.91	107052.9518	0.0030	2.41	204	107052.9522	0.0007	19.41	1263
22	27.91	107052.9522	0.0026	2.35	213	107052.9522	0.0005	17.86	1322
24	27.91	107052.9522	0.0026	2.24	216	107052.9522	0.0006	17.93	1341

gorithm can achieve the smallest Max_diff after certain number of iterations. Because the image qualities are almost unaffected by several pixels with relatively large errors, we terminate the DDMs by the absolute error of the numerical energy to save the computational costs. Besides, we observe that both PSNR and numerical energies converge to almost the same values, which means both DDMs converge to the same solution no matter how many subdomains are used. Visualized results in Figure 5.1 and Figure 5.5 further confirm our conclusion, in which one can not find any visual differences among the results with different numbers of subdomains with extremely small differences occurred on the interfaces.

Table 5.4: Inpainting results of image "Boat" and "Building".

Boat,$\tau_0 = 2.5, \lambda = 35$					Building,$\tau_0 = 2.5, \lambda = 20$				
N_{sub}	Energy	PSNR	Time	Iter	N_{sub}	Energy	PSNR	Time	Iter
2	7541.6319	33.20	18.45	544	2	19204.5282	33.97	66.35	405
6	7541.5922	33.20	4.84	592	8	19204.8664	33.98	17.43	496
10	7541.7190	33.21	3.82	614	14	19205.2722	33.98	6.80	499
12	7541.7599	33.22	3.50	626	20	19205.5932	33.98	5.21	526
16	7541.8194	33.22	3.00	664	24	19205.7250	33.97	4.98	554

In the following, we apply our non-overlapping DDM to inpainting and deblurring problems, where the same test images are used with missing domains as shown in Figure 5.6. For inpainting examples, the stopping conditions are provided as $e_n \leq 5 \times 10^{-6}$ and $e_n \leq 1 \times 10^{-6}$ for image "Boat" and "Building", respectively. Simultaneously, the inner loops of subdomains for both images are set as $e_n \leq 10^{-6}$ or nIn ≥ 100. As can be seen from Table 5.4, the performance of our algorithm on inpainting problems is consistent with denoising, where the virtual wall clock decreases as the number of subdomains keeps increasing. For deblurring problems, we degrade both image "Boat" and "Building" by a Gaussian blur kernel of size 3×3. The external loops are terminated by the relative

(a) Boat 512×512 (b) $N_{\text{sub}} = 2$ (c) $N_{\text{sub}} = 8$ (d) $N_{\text{sub}} = 16$

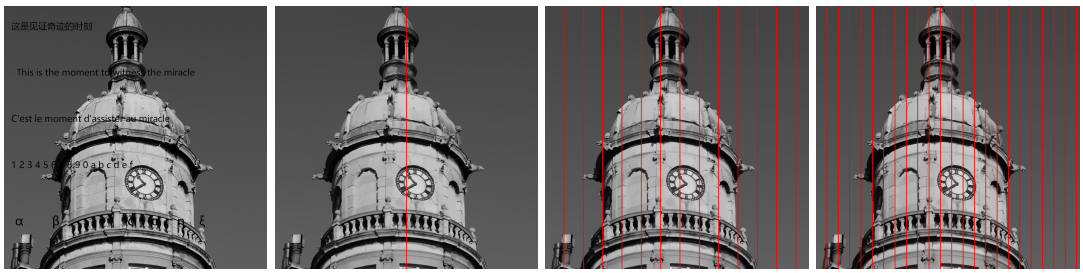

(e) Building1024 × 1024 (f) $N_{\text{sub}} = 2$ (g) $N_{\text{sub}} = 14$ (h) $N_{\text{sub}} = 24$

Figure 5.6: Inpainting images and results, where the red lines indicate the positions of interfaces Γ.

error $e_n \leq 10^{-6}$, while the stopping conditions are set as the same as inpainting for the inner loops. Though the values of PSNR and numerical energies in Table 5.5 are not as stable as the former experiments, which can be attributed to the differences of terminating conditions of external loops, the proficiency improvements brought by DDM are extraordinary. Furthermore, we provide the residual error of "Building" in Figure 5.7 with different numbers of subdomains. Although the residual error in the missing area is not as small as the denoising case, the distribution of error is obviously independent of the number of subdomains.

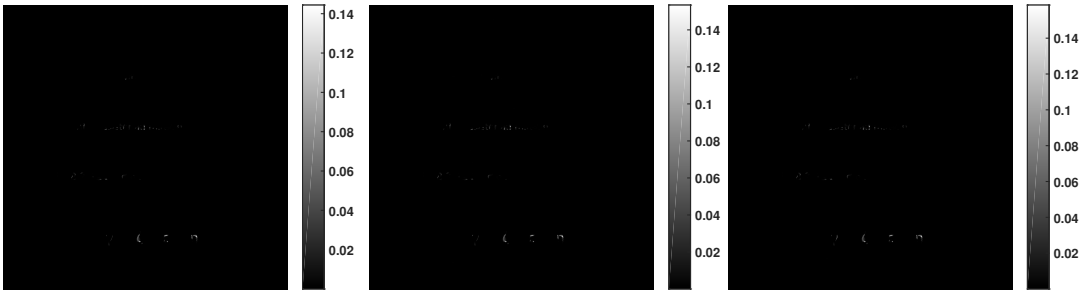

(a) $N_{\text{sub}} = 2$ (b) $N_{\text{sub}} = 14$ (c) $N_{\text{sub}} = 24$

Figure 5.7: Residual errors of image "Building" on image inpainting application with different numbers of sundomains.

Table 5.5: Deblurring results of image "Boat" and "Building".

Boat, $\tau_0 = 0.05, \lambda = 20$					Building, $\tau_0 = 0.05, \lambda = 20$				
N_{sub}	Energy	PSNR	Time	Iter	N_{sub}	Energy	PSNR	Time	Iter
2	17397.1502	27.93	21.45	499	2	202856.2680	27.14	100.37	623
6	17400.1234	27.92	5.69	510	8	202884.6530	27.14	27.80	672
10	17402.3245	27.91	4.40	548	14	202909.6712	27.14	11.53	721
12	17404.2672	27.90	4.13	566	20	202938.0442	27.14	8.75	744
16	17408.4268	27.90	3.25	590	24	202951.8130	27.14	7.95	750

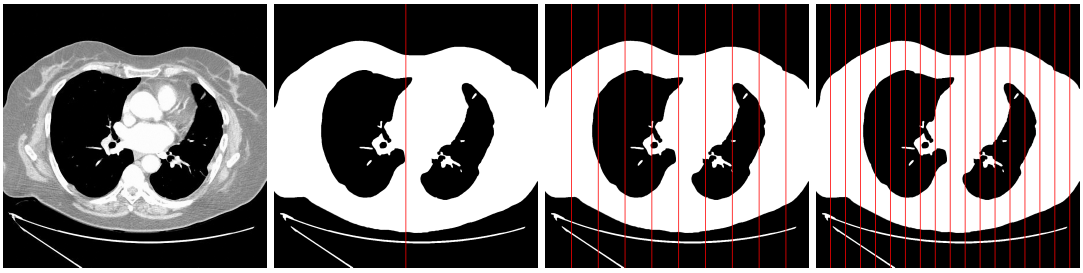

(a) Lung 1024×1024 (b) $N_{\text{sub}} = 2$ (c) $N_{\text{sub}} = 10$ (d) $N_{\text{sub}} = 18$

(e) Leaf 2048×2048 (f) $N_{\text{sub}} = 2$ (g) $N_{\text{sub}} = 14$ (h) $N_{\text{sub}} = 26$

Figure 5.8: Testing images for segmentation and the corresponding segmentation results obtained by the proposed non-overlapping DDM with different numbers of sundomains.

5.2. Image segmentation

Although the segmentation problem does not have a uniformly convex data fidelity term, which disables most acceleration algorithms, our algorithm is still applicable with fixed step sizes. Two test images "Lung" and "Leaf" in Figure 5.8 are chosen to evaluate the performance of our DDM. For segmentation, the inner loop is stopped using the maximal iteration number of 10, and the external loops are terminated by $E_n \leq 10^{-6}$ and $E_n \leq 5 \times 10^{-7}$ for image "Lung" and "Leaf", respectively. We compare our algorithm with Algorithm Duan16 for different combinations of images and numbers of subdomains. As shown in Table 5.6 and Table 5.7, our algorithm outperforms Algorithm Duan16 by reducing the outer iterations significantly. Pay attention that the values of Max_diff concerning image "Leaf" are much larger than denoising due to the lack of uniform convexity, while the residual error between the segmentation results obtained by our DDM and the ground

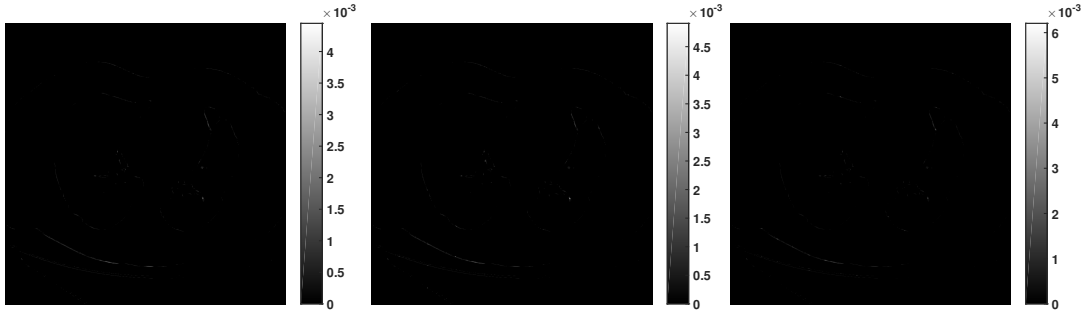

(a) $N_{\text{sub}} = 2$ (b) $N_{\text{sub}} = 10$ (c) $N_{\text{sub}} = 18$

Figure 5.9: Residual errors of image "Lung" on image segmentation application with different numbers of sundomains.

Table 5.6: Comparison results of Algorithm 3 and Algorithm Duan16 for Figure 5.8 (a).

Nsub	Li_Acc $\tau = \gamma = 0.5$				Duan16 $\tau = \gamma = 0.5$			
	Energy	Max_diff	Time	Iter	Energy	Max_diff	Time	Iter
2	22046.2572	0.0044	279.91	533	22046.1692	0.0015	212.25	782
6	22046.2574	0.0042	86.28	553	22046.1692	0.0014	67.51	796
10	22046.2572	0.0049	35.84	572	22046.1691	0.0022	34.18	814
14	22046.2570	0.0072	22.98	592	22046.1691	0.0020	19.50	814
18	22046.2573	0.0062	17.24	600	22046.1692	0.0016	12.65	840
22	22046.2572	0.0051	12.96	615	22046.1692	0.0016	11.15	868

truth u^* is acceptable for the image "Lung", as shown by Table 5.6 and Figure 5.9. As there is no visual difference between the results obtained by DDM and ground truth, we save the trouble of displaying the ground truth.

6. Conclusion

In this paper, we proposed the accelerated non-overlapping DDM for the total variation minimization models. Local problems on both interfaces and subdomains are small-size original minimization problems. Therefore, the acceleration technique can be applied to achieve an $O(1/n^2)$ convergence rate for image reconstruction problems, for which the data fidelity is uniformly convex. Besides, we developed a new convergent non-overlapping DDM for the convex Chan-Vese model. By comparing with state-of-art non-overlapping DDMs, we demonstrated the new one outperformed others by providing a fast convergence with the same step sizes and termination conditions, which coincides with the theoretical results. Possible further work includes design accelerated non-overlapping DDM for the Chan-Vese model based on more efficient local solvers such as the preconditioned and over-relaxed Douglas-Rachford splitting methods in [30].

Table 5.7: Comparison results of Algorithm 3 and Algorithm Duan16 for Figure 5.8 (e).

Nsub	Li_Acc $\tau=\gamma=1.5$				Duan16 $\tau=\gamma=1.5$			
	Energy	Max_diff	Time	Iter	Energy	Max_diff	Time	Iter
2	27442.7466	0.5340	684.67	290	27442.8698	0.7846	402.86	338
6	27442.7466	0.5340	205.51	290	27442.8698	0.7847	125.71	338
10	27442.7467	0.5340	114.56	290	27442.8699	0.7847	72.54	338
14	27442.7466	0.5343	75.33	289	27442.8701	0.7837	50.74	339
18	27442.7467	0.5360	55.82	289	27442.8701	0.7671	40.35	355
22	27442.7466	0.5338	36.88	290	27442.8697	0.7839	31.82	339
26	27442.7466	0.5362	30.85	289	27442.8696	0.7838	27.67	339
30	27442.7467	0.5358	22.71	289	27442.8702	0.7849	23.38	338
34	27442.7467	0.5340	14.58	290	27442.8701	0.7694	16.70	353

Acknowledgements

The authors would like to thank Prof Lee Chang-Ock for valuable discussion and providing the codes of [22] for comparison. The research was supported by NSFC 11701418, 12071345 and Major Science and Technology Project of Tianjin(18ZXRHSY00160) and the Recruitment Program of Global Young Expert. The work of H Chang was partially supported by the NSFC 11871372 and 11501413.

References

[1] Amir Beck and Marc Teboulle. A fast iterative shrinkage-thresholding algorithm for linear inverse problems. *SIAM Journal on Imaging Sciences*, 2(1):183–202, 2009.

[2] Xavier Bresson, Selim Esedoglu, Pierre Vandergheynst, Jean-Philippe Thiran, and Stanley Osher. Fast global minimization of the active contour/snake model. *Journal of Mathematical Imaging and Vision*, 28(2):151–167, July 2007.

[3] Antonin Chambolle. An algorithm for total variation minimization and applications. *Journal of Mathematical Imaging and Vision*, 20(1-2):89–97, 2004.

[4] Antonin Chambolle and Thomas Pock. A first-order primal-dual algorithm for convex problems with applications to imaging. *Journal of Mathematical Imaging and Vision*, 40(1):120–145, 2011.

[5] Antonin Chambolle and Thomas Pock. On the ergodic convergence rates of a first-order primal–dual algorithm. *Mathematical Programming*, 159(1):253–287, 2016.

[6] Tony F Chan, Selim Esedoglu, and Mila Nikolova. Algorithms for finding global minimizers of image segmentation and denoising models. *SIAM Journal on Applied Mathematics*, 66(5):1632–1648, 2006.

[7] Tony F Chan and Luminita A Vese. Active contours without edges. *IEEE Transactions on Image Processing*, 10(2):266–277, 2001.

[8] Huibin Chang, Xue-Cheng Tai, Li-Lian Wang, and Danping Yang. Convergence rate of overlapping domain decomposition methods for the rudin-osher-fatami model based on a dual formulation. *SIAM Journal on Imaging Sciences*, 8:564–591, 2015.

[9] Peijun Chen, Jianguo Huang, and Xiaoqun Zhang. A primal dual fixed point algorithm for convex separable minimization with applications to image restoration. *Inverse Problems*, 29(2):025011, 2013.
[10] Yunmei Chen, Guanghui Lan, and Yuyuan Ouyang. Optimal primal-dual methods for a class of saddle point problems. *SIAM Journal on Optimization*, 24(4):1779–1814, 2014.
[11] Laurent Condat. A direct algorithm for 1D total variation denoising. *IEEE Signal Processing Letters*, 20(11):1054–1057, 2013.
[12] Laurent Condat. A generic proximal algorithm for convex optimization—application to total variation minimization. *IEEE Signal Processing Letters*, 21(8):985–989, 2014.
[13] Victorita Dolean, Pierre Jolivet, and Frédéric Nataf. *An introduction to domain decomposition methods: algorithms, theory, and parallel implementation*. SIAM, 2015.
[14] Yuping Duan, Huibin Chang, and Xue-Cheng Tai. Convergent non-overlapping domain decomposition methods for variational image segmentation. *Journal of Scientific Computing*, 69(2):532–555, 2016.
[15] Yuping Duan and Xue-Cheng Tai. Domain decomposition methods with graph cuts algorithms for total variation minimization. *Advances in Computational Mathematics*, 36(2):175–199, 2012.
[16] Massimo Fornasier, Andreas Langer, and Carola-Bibiane Schönlieb. A convergent overlapping domain decomposition method for total variation minimization. *Numerische Mathematik*, 116(4):645–685, 2010.
[17] Massimo Fornasier and Carola-Bibiane Schönlieb. Subspace correction methods for total variation and ℓ_1-minimization. *SIAM Journal on Numerical Analysis*, 47(5):3397–3428, January 2009.
[18] Tom Goldstein and Stanley Osher. The split bregman method for L1-regularized problems. *SIAM Journal on Imaging Sciences*, 2(2):323–343, 2009.
[19] Michael Hintermüller and Andreas Langer. Non-overlapping domain decomposition methods for dual total variation based image denoising. *Journal of Scientific Computing*, 62(2):456–481, 2015.
[20] Andreas Langer and Fernando Gaspoz. Overlapping domain decomposition methods for total variation denoising. *SIAM Journal on Numerical Analysis*, 57(3):1411–1444, 2019.
[21] Andreas Langer, Stanley Osher, and Carola-Bibiane Schönlieb. Bregmanized domain decomposition for image restoration. *Journal of Scientific Computing*, 54(2-3):549–576, 2013.
[22] Chang-Ock Lee and Changmin Nam. Primal domain decomposition methods for the total variation minimization, based on dual decomposition. *SIAM Journal on Scientific Computing*, 39(2):B403–B423, 2017.
[23] Chang-Ock Lee, Changmin Nam, and Jongho Park. Domain decomposition methods using dual conversion for the total variation minimization with L^1 fidelity term. *Journal of Scientific Computing*, 78(2):951–970, 2019.
[24] Chang-Ock Lee and Jongho Park. Fast nonoverlapping block jacobi method for the dual rudin–osher–fatemi model. *SIAM Journal on Imaging Sciences*, 12(4):2009–2034, 2019.
[25] Chang-Ock Lee and Jongho Park. Recent advances in domain decomposition methods for total variation minimization. *Journal of the Korean Society for Industrial and Applied Mathematics*, 24(2):161–197, 2020.
[26] Jan Lellmann, Dirk Breitenreicher, and Christoph Schnörr. Fast and exact primal-dual iterations for variational problems in computer vision. In *European conference on computer vision*, pages 494–505, 2010.
[27] Charles A Micchelli, Lixin Shen, and Yuesheng Xu. Proximity algorithms for image models: denoising. *Inverse Problems*, 27(4):045009, 2011.

[28] Yu Nesterov. Smooth minimization of non-smooth functions. *Mathematical Programming*, 103(1):127–152, 2005.

[29] Leonid I. Rudin, Stanley Osher, and Emad Fatemi. Nonlinear total variation based noise removal algorithms. *Physica D: Nonlinear Phenomena*, 60(1-4):259–268, 1992.

[30] Hongpeng Sun, Xuecheng Tai, and Jing Yuan. Efficient ADMM and splitting methods for continuous min-cut and max-flow problems. *arXiv preprint arXiv:2004.11227*, 2020.

[31] Xue-Cheng Tai and Jinchao Xu. Global and uniform convergence of subspace correction methods for some convex optimization problems. *Mathematics of Computation*, 71(237):105–124, 2002.

[32] Shanshan Tang and Haijun Yu. Application of bounded total variation denoising in urban traffic analysis. *East Asian Journal on Applied Mathematics*, 9:622–642, 2019.

[33] C. R. Vogel and M.E. Oman. Fast, robust total variation-based reconstruction of noisy, blurred images. *IEEE Transactions on Image Processing*, 7(6):813–824.

[34] Chunlin Wu and Xue-Cheng Tai. Augmented lagrangian method, dual methods and split-bregman iterations for ROF, vectorial TV and higher order models. *SIAM Journal on Imaging Sciences*, 3:300–339, 2010.

[35] Jinchao Xu. Iterative methods by space decomposition and subspace correction. *SIAM Review*, 34(4):581–613, 1992.

[36] Jing Xu, Xue-Cheng Tai, and Li-Lian Wang. A two-level domain decomposition method for image restoration. *Inverse Problem & Imaging*, 4(3):523–545, 2010.

[37] Jing Yuan, Egil Bae, Xue-Cheng Tai, and Yuri Boykov. A continuous max-flow approach to potts model. In *European Conference on Computer Vision*, pages 379–392, 2010.